Int. J. Heat Mass Transfer. Vol. 29, No. 3, pp. 369–379, 1986
Printed in Great Britain

0017–9310/86 $3.00 + 0.00

Local and average natural convection Nusselt numbers for a uniformly heated, shrouded or unshrouded horizontal plate

E. M. SPARROW and C. K. CARLSON
Department of Mechanical Engineering, University of Minnesota, Minneapolis, MN 55455, U.S.A.

(*Received* 12 *July* 1985 *and in final form* 23 *September* 1985)

Abstract—Experiments were performed to determine the local and average natural convection heat transfer characteristics for a uniformly heated, upward-facing horizontal plate shrouded by a parallel adiabatic surface situated above the plate. Three parameters were varied during the experiments, including the dimensionless height of the interplate gap (the no-shroud case serving as the upper limit), the dimensionless heating rate (the Rayleigh number), and the configuration of the surroundings (absence or presence of an obstruction and of supplemental insulation). Air was the heat transfer medium. The local Nusselt number was highest at the edge of the heated plate and decreased along the plate surface; at the center of the plate, the Nusselt number was about one-third of that at the edge. The local Nusselt number distributions, when normalized by the corresponding average Nusselt number, were found to be universal (i.e. independent of the parameters) for gap heights above a threshold value. Both the local and average Nusselt numbers were depressed at small gap heights but rebounded rapidly with increasing gap height. A critical gap height was found such that for values exceeding it, the average Nusselt number was independent of the presence or absence of the shroud.

INTRODUCTION

THE HEATED horizontal plate is one of the basic configurations for which natural convection heat transfer results are generally reported in textbooks, handbooks, and compilations. The available experimental literature is limited to average Nusselt numbers corresponding to the uniform wall temperature boundary condition, with the most often cited references encompassing experiments on heat transfer [1], naphthalene sublimation [2], and electrochemical mass transfer [3]. In practice, interactions between a heated horizontal plate and other surfaces are frequently encountered, and it is such interactions which constitute the main theme of the present investigation. The aforementioned basic configuration of a single (non-interacting) heated plate was also investigated, since local heat transfer coefficients and uniform surface heat flux, both features of the present work, have not been previously dealt with for that case.

A schematic diagram depicting the physical problem is presented in Fig. 1(a). The figure shows a uniformly heated horizontal plate of width W. Directly above the plate and separated from it by an air space of height H is an insulated surface of identical planform dimensions. Air from the surroundings is free to enter or leave the space through the openings ABCD and A′B′C′D′. The experiments were conducted so as to obtain results that are independent of the longitudinal coordinate y and, to help fulfill this objective, airflow through the faces BCC′B′ and ADD′A′ was suppressed.

The buoyancy created by the heated plate induces a flow pattern whereby air from the surroundings is drawn into the opening ABCD adjacent to the plate surface. This air stream moves inward along the plate (i.e. in the positive x-direction) while tending to rise due to buoyancy. The farthest inward penetration of the stream is to $x = W/2$, where it collides with an identical stream which enters through the opposite opening A′B′C′D′. The upwelling air encounters the insulated upper surface, along which it flows toward the opening ABCD and then out into the surroundings (a similar outflow occurs through the opening A′B′C′D′). Thus, in broad terms, the flow pattern can be thought of as consisting of two U-shaped loops, one in the space between $x = 0$ and $W/2$ and the other in the space between $x = W/2$ and W. This flow pattern will give rise to x-dependent variations of the local heat transfer coefficient, with symmetry about $x = W/2$.

Measurements were made to determine the local natural convection Nusselt number as a function of position x/W across the width of the uniformly heated plate. Average Nusselt numbers were also evaluated from the local measurements. These results were obtained as a function of the dimensionless gap height H/W and of a modified Rayleigh number which served to characterize the heating rate. The gap height ranged from $H/W = 0.16$ to ∞ in seven steps, with the $H/W = \infty$ case corresponding to the absence of the insulated upper surface.

The experimental work was supplemented by an analysis of the complex radiative interchange between the participating surfaces and with the surroundings. The analysis made use of a specular–diffuse model, in recognition of the radiation properties of the highly polished surface of the heated plate (a polished surface was used to obtain low emissivity). Furthermore, in view of the relatively low natural convection heat transfer coefficients that are characteristic of the investigated configuration, measures were taken to avoid extraneous heat losses. Losses from the exposed

NOMENCLATURE

g	acceleration of gravity
H	height of interplate gap
h	local heat transfer coefficient, equation (4)
$\bar{h}$	average heat transfer coefficient, equation (6)
I_x	local incident radiative flux
k	thermal conductivity
Nu	local Nusselt number, hW/k
$\overline{Nu}$	average Nusselt number, $\bar{h}W/\bar{k}$
Pr	Prandtl number
q_{cond}	local conductive heat flux into insulation bed
q_{Ohm}	local heat flux input due to Ohmic heating
q_{rad}	local radiative heat flux
q_x	local natural convection heat flux
$\bar{q}$	average natural convection heat flux
Ra^*	local modified Rayleigh number, equation (11)
$\overline{Ra}^*$	plate-average modified Rayleigh number, equation (7)
$\overline{Ra}$	plate-average Rayleigh number, equation (13)
T_f	local film temperature, $\frac{1}{2}(T_{wx}+T_\infty)$
$\bar{T}_f$	average film temperature, $\frac{1}{2}(\bar{T}_w+T_\infty)$
T_{wx}	local plate temperature
$\bar{T}_w$	average plate temperature
T_∞	ambient temperature
W	width of heated plate
x	coordinate across plate width at mid-line
y	coordinate along plate length.

Greek symbols

α	absorptivity
β	coefficient of thermal expansion
ε	emissivity
θ	reduced temperature, equation (9)
ν	kinematic viscosity
σ	Stefan–Boltzmann constant.

Other symbol

$\bar{}$	fluid property evaluated at $\bar{T}_f$.

edges AB, CD, A′B′, and C′D′ were eliminated by making the heated plate from a very thin metallic foil, the edge area of which was negligible. Furthermore, heat losses from the lower face of the plate were virtually eliminated by suspending it over a bed of insulation whose thermal conductivity is less than that of air.

To provide a broad range of heat transfer information, three versions of the problem described in the foregoing paragraphs were investigated. In the first version, the openings ABCD and A′B′C′D′ looked out on virtually unbounded and unobstructed surroundings. In the second version, the heated plate is framed by a coplanar adiabatic surface, as depicted in Fig. 1(b). The presence of the frame prevented air from being drawn into the opening from below. The third version is actually a variant of the second, wherein the exposed faces of the insulation bed situated below the heated plate were, themselves, additionally insulated.

The most relevant experimental literature has already been mentioned. There is some available analytical work [4, 5] which, although only loosely related to the configurations investigated here, is worthy of mention. That work dealt with natural convection along a heated, semi-infinite, horizontal

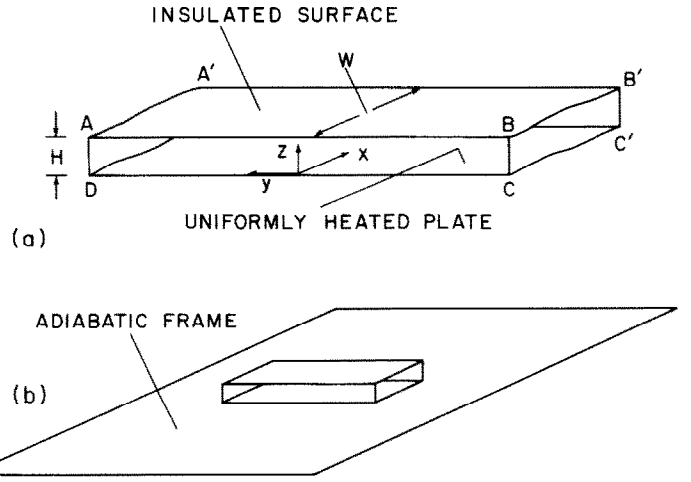

FIG. 1. Uniformly heated plate shrouded from above by a parallel, insulated surface.

plate. In terms of Fig. 1(a), this corresponds to $H = \infty$ and $W = \infty$, with a boundary-layer flow moving from the edge CD along the plate in the positive x-direction. This flow pattern differs from that of the experiments, where oppositely directed boundary layers are initiated from the leading edges CD and C'D'. Comparisons will be made wherever possible between the present experimental data and the literature.

EXPERIMENTAL APPARATUS AND PROCEDURE

The description of the experimental apparatus is facilitated by reference to the schematic side view presented in Fig. 2. To provide continuity with the problem statement conveyed by Fig. 1(a), the same letters, ABCD, have been appended to the near-side opening of the air gap in Fig. 2. The apparatus illustrated in the figure is the basic version, without either the frame or the supplemental insulation beneath the frame. These features will be considered later.

Apparatus

The heart of the apparatus is a 0.00254-cm-thick, electric-current-carrying sheet of stainless steel which served as the uniformly heated plate. The stainless steel sheet was suspended horizontally between two support blocks that were made of closed-pore, extruded polystyrene insulation (Styrofoam) that could be machined to close tolerances with a smooth surface finish. As seen in Fig. 1, each support block was fabricated with a flat, raised platform on which the stainless steel sheet lay and to which the sheet was firmly affixed with epoxy cement. Outboard of the platform, each block was downstepped to provide a seat for a specially designed, two-piece aluminium bus bar whose clamplike jaw grasped the steel sheet uniformly all along its width. The bottom face of each support block was cemented to a wooden baseplate.

Prior to the installation of the stainless steel sheet, an open-topped, rectangular enclosure was created beneath the plane of the sheet to house silica aerogel powder insulation, the thermal conductivity of which is about 85% of that of air. The wooden baseplate served as the base of the enclosure, while the face-to-face surfaces of the support blocks served as the end walls. The long sidewalls of the enclosure were made of tightly stretched 0.00127-cm-thick polyethylene anchored to the support blocks and the baseplate. At the top, the enclosure was capped by the stainless steel sheet, with the seal being accomplished by thin, highly adhesive tape attached to the inner face of the polyethylene and to the lower face of the sheet. The thus-housed insulation bed was 9.5 cm deep.

The use of sidewalls of virtually zero thickness (i.e. the polyethylene) enabled the aerogel insulation to extend out to the very edges of the stainless steel sheet (where it was most needed). Furthermore, the transparency of the polyethylene permitted the fullness of the insulation in the enclosure to be visually verified. Had more conventional (i.e. thicker) sidewalls been used, the geometry of the openings ABCD and A'B'C'D' might have been altered and additional heat loss paths created.

A pair of spacer blocks, each machined to rest atop one of the bus bars and on the adjacent stepped-down portion of the support block, served to set the height H of the air gap. The other function of the spacer blocks was to close the ends of the air gap and thereby suppress airflow through the ends, thus aiding in the attainment of two-dimensionality. The spacer blocks were made of Styrofoam, and the surfaces which faced the air gap were covered with plasticized, self-adhering contact paper.

In total, seven sets of spacer blocks were used, six in conjunction with the insulated upper wall of the air gap and the seventh in the absence of the upper wall. The resulting dimensionless heights of the air gap were

$$H/W = 0.16, 0.21, 0.26, 0.31, 0.52, 0.70 \text{ and } \infty. \quad (1)$$

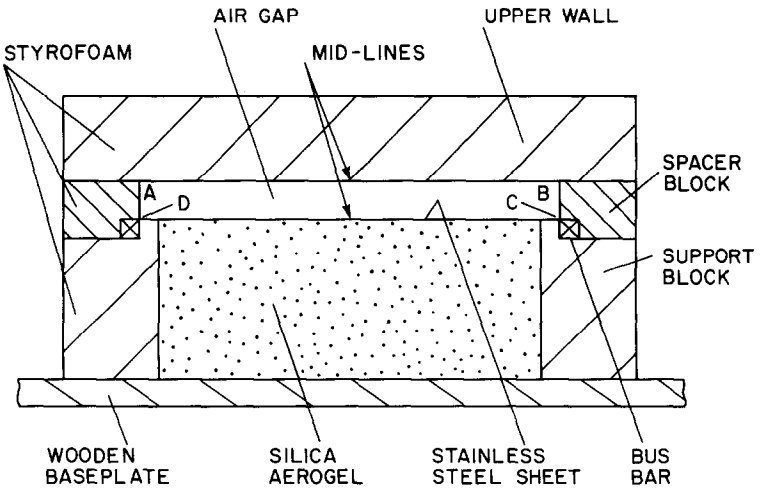

FIG. 2. Side view of the experimental apparatus.

In the $H/W = \infty$ case, with no upper wall to support, the spacer blocks were employed to suppress airflow into or out of the ends of the air gap (for that case, the block height was $1.6W$).

The upper bounding wall of the air gap was made from a 5.08-cm-thick Styrofoam block having a width equal to that of the stainless steel sheet. The edge AB of the block was positioned directly above the edge DC of the sheet, and similarly for the edges A'B' and D'C'. All of the exposed surfaces of the block were covered with plasticized contact paper. Six thermocouples were installed at the wall surface which bounded the air gap. The thermocouples were deployed across the width of the surface along a line midway between the closed ends of the gap. That line, hereafter designated as the mid-line, is indicated in Fig. 2.

Heated plate

With the overall description of the apparatus now completed, attention will be turned to the details of the uniformly heated plate. The 0.00254-cm-thick stainless steel sheet which served as the heated plate had a width W of 7.62 cm and an exposed length (between the closed ends of the gap) of 25.4 cm. The sheet was instrumented on its lower surface with thermocouples and with voltage taps in order to facilitate the determination of local heat transfer results. All measurements were made in the region where two-dimensionality was believed to prevail, i.e. away from the closed ends of the gap.

The thermocouple and voltage tap wires and their mode of installation were chosen with a view to minimizing the disturbance of the temperature and voltage distributions in the stainless steel sheet. Small diameter (0.00762 cm), low-thermal-conductivity wire was used, respectively chromel/constantan for the thermocouples and constantan for the voltage taps. The attachment was accomplished with epoxy (copper-filled for the tap attachment), applied in minimal amounts. The lead wires were laid along the expected isotherms.

Ten thermocouples were attached to the sheet. Eight of these were deployed across the width of the sheet along the mid-line, while the other two were displaced symmetrically on either side of the mid-line to verify two-dimensionality. There were four voltage taps, two to either side of the mid-line and respectively 5.08 and 10.16 cm from it.

To minimize the effects of thermal radiation, the exposed surface of the stainless steel sheet was painstakingly hand polished to a high luster. The polishing was performed using a succession of lapping compounds, terminating with a 1200-grit compound, and the polishing procedure (polishing stroke direction and duration of polishing period) was optimized by checking the reflectivity obtained for several candidate procedures. The reflectivity measurements were made at seven representative surface locations with a Gier–Dunkle heated-cavity reflectometer having radiation source temperatures of 25° and 100°C. The emissivity deduced from these measurements was 0.10.

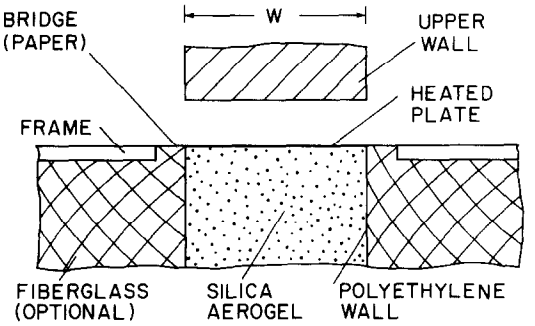

FIG. 3. End-view cross section of the experimental apparatus cut through the mid-line.

Further information about the fabrication of the experimental apparatus is available in ref. [6].

Frame and supplemental insulation

The version of the apparatus which incorporated an adiabatic frame has been illustrated schematically in Fig. 1(b) and will now be elaborated. To facilitate the description, an end-view cross section of the apparatus, cut through the mid-line, is pictured in Fig. 3. As seen there, the apparatus proper (i.e. the heated plate, upper wall, and silica aerogel insulation bed) is flanked at either side by a horizontal frame made of 0.635-cm-thick, paper-covered, foam-filled art board, the upper surface of which was positioned to be coplanar with the exposed surface of the heated plate. To avoid heat conduction between the frame and the edges of the plate, a 1.27 cm clearance gap was left between each tip of the frame and the adjacent plate edge. The clearance gap was bridged by a sheet of 0.007-cm-thick paper, thereby providing a continuous surface for the airflow. The paper was fixed in place by tape applied from below.

The horizontal dimensions of the frame were sufficiently large so that they were, in effect, infinite. Therefore, the presence of the frame should affect the pattern of fluid flow by preventing air from being drawn into the opening from below.

With the frame in place, another variant of the apparatus was obtained by filling the space below the frame with fiberglass insulation, as seen in Fig. 3. The supplemental insulation served to prevent heat losses from the polyethylene wall which bounded the silica aerogel insulation enclosure, especially from that part of the wall adjacent to the heated plate.

Laboratory setting and experimental procedure

The experiments were conducted in a laboratory which is actually a room within a room, with 30.5-cm-thick cork walls to provide thermal isolation. The laboratory is in a deep basement, is unheated, and no ventilating ducts pass through its walls. Temperature stability is further enhanced by the presence of a substantial amount of distributed thermal mass. The power supply and the other instrumentation for the

experiments were situated outside the laboratory. The laboratory was sealed and unlighted during the entire 24-h duration of a data run.

To measure the laboratory ambient temperature relevant to the experiment, thermocouples were positioned in the expected path of the air drawn into the apparatus. The thermocouples were shielded from the radiation emitted by the heated plate.

Power was supplied to the heated plate from a DC source having 0.02% or better voltage stability over a 24-h period. The thermocouple and current shunt voltages were read to 1 μV, while the inter-tap voltage drops were read to four significant figures.

DATA REDUCTION

Local Nusselt numbers were evaluated as a function of the transverse coordinate x along the mid-line of the heated plate. The evaluation was performed at locations x at which the plate temperature was measured.

The local convective heat flux q_x was obtained from the electric power input by subtraction of the conduction and radiation heat losses. The uniformity of the voltage drop along the length of the plate evidenced by the voltage taps, supplemented by the transverse uniformity of the voltage measured during traverses made prior to the installation of the plate in the apparatus, affirmed the uniformity of the Ohmic dissipation. By utilizing the measured electric current flow, the voltage drop between the two taps nearest the mid-line, and the exposed surface area of the plate between these taps, the local Ohmic heat flux q_{Ohm} was obtained. Then,

$$q_x = q_{\text{Ohm}} - q_{\text{cond}} - q_{\text{rad}}. \tag{2}$$

The quantity q_{cond} is the local conduction heat flux from the plate through the silica aerogel insulation to the baseplate. If k_{ins} denotes the thermal conductivity of the aerogel insulation [7] and H_{bed} (=9.5 cm) is the height of the insulation bed,

$$q_{\text{cond}} = k_{\text{ins}}(T_{\text{wx}} - T_{\text{base}})/H_{\text{bed}}. \tag{3}$$

In this equation, T_{wx} is the plate temperature at location x, while T_{base} is the measured temperature at the upper surface of the baseplate [note that k_{ins} was evaluated at $\frac{1}{2}(T_{\text{wx}} + T_{\text{base}})$]. The determination of the radiation heat flux is quite complex and will be described later.

With q_x from equation (2), the local heat transfer coefficient and Nusselt number were evaluated as

$$h = q_x/(T_{\text{wx}} - T_\infty), \quad Nu = hW/k \tag{4}$$

in which k, the thermal conductivity of air, corresponds to the local film temperature $T_{\text{f}} = \frac{1}{2}(T_{\text{wx}} + T_\infty)$. The plate width W was used as the characteristic length in the local Nusselt number rather than the local coordinate x in order that the x-dependence of Nu would closely reflect the x-dependence of h.

Average heat transfer coefficients and Nusselt numbers were also determined. To this end, let

$$\bar{q} = \left[\int_0^W q_x \, dx\right] \Big/ W, \quad \bar{T}_{\text{w}} = \left[\int_0^W T_{\text{wx}} \, dx\right] \Big/ W \tag{5}$$

in which the integration was carried out numerically [6]. Then, with $\bar{q}$ and $\bar{T}_{\text{w}}$,

$$\bar{h} = \bar{q}/(\bar{T}_{\text{w}} - T_\infty), \quad \overline{Nu} = \bar{h}W/\bar{k}. \tag{6}$$

Natural convection Nusselt number results are customarily parameterized by the Rayleigh number. In cases where the heat flux is prescribed (in contrast to prescribed wall temperature), it is appropriate to use a modified Rayleigh number which is based on the heat flux rather than on the wall-to-ambient temperature difference that appears in the conventional Rayleigh number. Taking into account the average heat flux $\bar{q}$ and the average thermophysical properties of air (all evaluated at $\bar{T}_{\text{f}}$), the plate-average modified Rayleigh number will be defined as

$$\overline{Ra}^* = (g\bar{\beta}\bar{q}W^4/\bar{\nu}^2\bar{k})\overline{Pr} \tag{7}$$

and used to parameterize the experimental results. Other versions of the Rayleigh number appropriate to the comparison of the present results to literature information will be introduced later as needed.

Analysis of radiative heat transfer

The objective of the radiation analysis was to determine q_{rad} at locations x along the mid-line where temperature measurements were made. At any such location x, q_{rad} is the net of the emitted and absorbed fluxes of radiation, so that

$$q_{\text{rad}} = \varepsilon\sigma T_{\text{wx}}^4 - \alpha I_x \tag{8}$$

where I_x is the radiation incident at x per unit time and unit area. I_x is made up of both direct contributions (emission at the upper wall of the air gap, emission at the walls which close the ends of the gap, and radiation from the surroundings which streams into the gap) and indirect contributions (reflections at all of the bounding walls of the gap). Included in the latter is radiation emitted by the heated plate which, after single or multiple reflections, returns to the plate.

The special feature of the problem is that the heated plate, because of its highly polished surface, reflects in a specular (i.e. mirror-like) manner. This characteristic precludes the use of standard calculation methods which are based on diffusely reflecting and emitting surfaces.

To simplify the analysis without in any way affecting the accuracy of the results, the temperature scale will be shifted according to the definition

$$\theta^4 = T^4 - T_\infty^4. \tag{9}$$

In the θ temperature scale, the ambient is at absolute zero and is nonradiating, so that no further consideration need be given to radiation streaming into the gap from the surroundings. Furthermore, the angle factor between a mid-line x-location and the end walls is very small and the surface area of the end walls is

also small, with the result that these walls have an insignificant influence on the q_{rad} values being sought. For this reason and also to simplify the analysis, the end walls were, in effect, eliminated from the problem by assuming that they are black and at temperature T_∞ (i.e. $\theta = 0$).

Both the heated plate and the upper wall of the air gap are nonisothermal surfaces with known (measured) x-dependent temperature distributions. Each surface was subdivided into an array of longitudinal isothermal strips and the appropriate angle factors determined. With the angle factors between an elemental area at x and the individual strips on the upper wall, the direct contribution of the upper-wall emission to I_x was evaluated.

A portion of the emission from the upper wall, after specular reflection at the heated plate, returns to the upper wall where, in part, it is diffusely reflected. In addition, radiation emitted at the heated plate is, in part, diffusely reflected at the upper wall. For computational convenience, the two diffusely reflected streams were merged and followed through subsequent reflections. A portion of the merged stream returns to the heated plate, where a part is absorbed (in particular, at x) and another part is specularly reflected back to the upper wall where it is partially diffusely reflected. This reflected radiation is partially absorbed at the heated plate, and so on and so forth. If a tally is kept of the successive absorptions of radiation at location x on the heated plate, a summable geometric series results. The sum of the series is added to I_x.

With I_x thus determined, q_{rad} follows from equation (8). The specular reflections were dealt with using the image method of refs. [8] and [9], and the execution of the radiation analysis described in the foregoing paragraphs is detailed in a step-by-step manner in [6]. The emissivity of the upper wall was measured to be 0.855, while, as previously noted, that of the heated plate is 0.10. Reflectivity and absorptivity values needed in the analysis were obtained from the aforementioned emissivities by employing the gray-body model.

RESULTS AND DISCUSSION

Local Nusselt numbers

Representative distributions of the local Nusselt number across the width of the heated plate are presented in Fig. 4. Each of the local distributions is normalized by the corresponding average Nusselt number, yielding the $Nu/\overline{Nu}$ ratio. This ratio is plotted as a function of the dimensionless cross-plate coordinate $x/(W/2)$ measured from one of the free edges of the plate [see Fig. 1(a) for definition of coordinates]. Note that because of symmetry, it is only necessary to cover the range from $x = 0$ to $x = W/2$, and this is reflected in the abscissa of Fig. 4.

Figure 4 conveys results for four of the seven dimensionless gap heights which were investigated (namely, $H/W = 0.16, 0.26, 0.52$ and ∞) and for three of the six dimensionless heating rates $\overline{Ra}^*$ (the lowest, the highest, and an intermediate value). These cases will be sufficient to convey the essential message of the figure (results for the other cases are available in ref. [6]).

The results for each H/W are referred to separate abscissa scales, the origins of which are successively shifted to the right to avoid overlap. As indicated in the legend at the lower right in the figure, $Nu/\overline{Nu}$ results are given for both the no-frame and framed configurations, the latter without supplemental insulation. The individual legends for each H/W describe the $\overline{Ra}^*$ parameterization, except for those cases where $Nu/\overline{Nu}$ is independent of $\overline{Ra}^*$, for which a black circle data symbol is used.

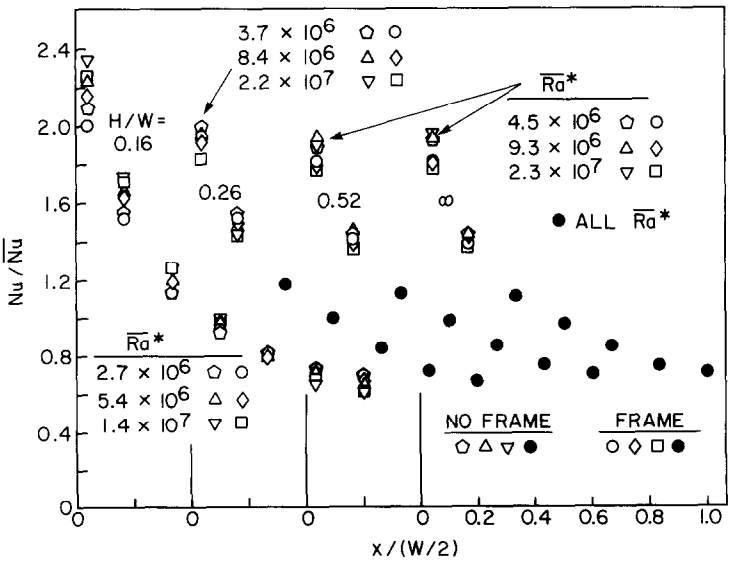

FIG. 4. Effect of heating rate $\overline{Ra}^*$ and frame vs no-frame configuration on the distributions of the normalized local Nusselt number $Nu/\overline{Nu}$.

The figure shows that for all of the operating and geometrical conditions, the local Nusselt number attains its highest value at the edge of the plate ($x = 0$ or $x = W$) and decreases monotonically in the direction from the edge toward the center of the width ($x = W/2$). The extent of the decrease is appreciable, with the edge-adjacent value of Nu being about three times as large as the value at the center. Owing to the near-uniformity of the convective heat flux, the decrease in Nu reflects a corresponding increase in the plate surface temperature, with the point at the center of the width being the hot spot.

The aforementioned decrease in the local Nusselt number is readily rationalized in terms of the growth of the thermal and hydrodynamic boundary layers which generally occurs when a fluid moves across a surface. In the present problem, other factors modify the boundary-layer growth along the heated plate and, presumably, affect the dropoff of the Nusselt number. One of these is the presence of two opposing streams, one moving across the plate from the edge at $x = 0$ toward the center of the width and the other moving toward the center from the edge at $x = W$. The collision of these streams causes the flow to lift off the plate, with an accompanying pre-liftoff thickening of the boundary layer. On the other hand, the collision should give rise to enhanced mixing. Another factor which is expected to thicken the boundary layer is the upward component of buoyancy. In the case of small gap heights, the oppositely directed flow along the upper wall of the gap should also contribute to retarding the fluid motion along the heated plate.

The other noteworthy feature of Fig. 4 is the excellent correlation of the local Nusselt number distributions which occurs when they are normalized by the average Nusselt number. Aside from the smallest gap height ($H/W = 0.16$) and the edge-adjacent station for the other gaps, the $Nu/\overline{Nu}$ values are virtually independent of the modified Rayleigh number $\overline{Ra}^*$ and of the presence or absence of a frame. This finding adds appreciable generality to the results.

Even for the smallest gap, the deviations from a mean line passed through the data are, at most, about 8%. The spread rapidly diminishes with increasing gap height so that, for most practical purposes, the $Nu/\overline{Nu}$ distribution for each gap height can be regarded as universal. For the larger gaps, the only departure from universality is a $\pm 5\%$ spread at the edge-adjacent point which reflects the presence or the absence of a frame, but there is no dependence on $\overline{Ra}^*$.

Information similar to that of Fig. 4, but bringing together the results for the frame and frame/insulation cases, is presented in Figs. 5.8–5.11 of ref. [6]. The trends in those figures are identical to those of Fig. 4—a moderate spread at the smallest gap height which dies away as the gap increases, with only a slight spread remaining at the edge-adjacent station. Therefore, the aforementioned universal nature of the $Nu/\overline{Nu}$ distributions is still further generalized.

The quantitative dependence of the $Nu/\overline{Nu}$ distributions on the gap height H/W, although implicit in Fig. 4, is more readily assessed with the aid of Fig. 5. There, for each of the three investigated configurations (no frame, frame, and frame/insulation), $Nu/\overline{Nu}$ is plotted as a function of $x/(W/2)$ for parametric values of H/W. To avoid overlap, the results for each configuration are referred to a separate abscissa scale. For concreteness, the results presented in the figure are for $\overline{Ra}^* \cong 6 \times 10^6$. However, in view of the demonstrated insensitivity of the $Nu/\overline{Nu}$ distributions to $\overline{Ra}^*$, the figure can be regarded as being applicable to any $\overline{Ra}^*$ om the investigated range.

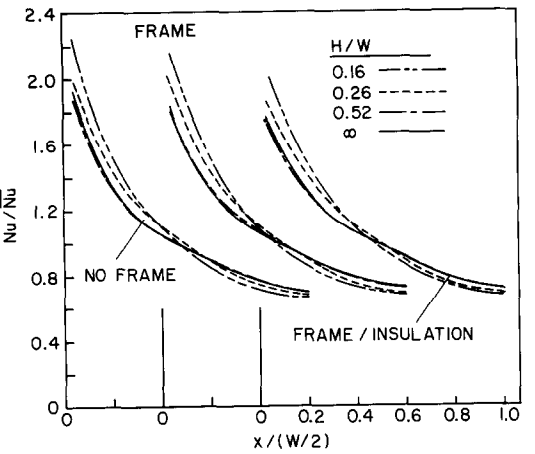

FIG. 5. Effect of gap height H/W on the distributions of the normalized local Nusselt number $Nu/\overline{Nu}$ ($\overline{Ra}^* = 6 \times 10^6$).

As seen from the figure, the lay of the curves is identical for the three configurations. In general, the greatest sensitivity of the $Nu/\overline{Nu}$ distributions to the gap height occurs at small heights; for larger gap heights (i.e. $H/W > 0.5$), $Nu/\overline{Nu}$ is independent of height. Thus, upon taking account of both Figs. 4 and 5, it can be concluded that for $H/W > 0.5$, the $Nu/\overline{Nu}$ distributions are truly universal—independent of $\overline{Ra}^*$, of H/W, and of the presence or absence of a frame (with or without supplemental insulation).

Further inspection of Fig. 5 shows that $Nu/\overline{Nu}$ is more responsive to gap height at stations near the edge of the plate than away from the edge. In particular, for stations between $x/(W/2) = 0.4$ and 1, the spread of $Nu/\overline{Nu}$ with H/W is sufficiently small so that, for most purposes, a mean line threaded through the plotted curves could be regarded as universal for all H/W.

The presentation of the local Nusselt number data in the $Nu/\overline{Nu}$ format, while leading to the various generalizations described in the foregoing paragraphs, precludes an assessment of the effect of the parameters on the actual Nu values. This information is provided in Fig. 6, where Nu is plotted as a function of $x/(W/2)$ for the no-frame, frame, and frame/insulation configurations. The data for each configuration are parameterized by the same H/W values as in the preceding figures, and curves have been passed through the data to provide continuity. Although the plotted results

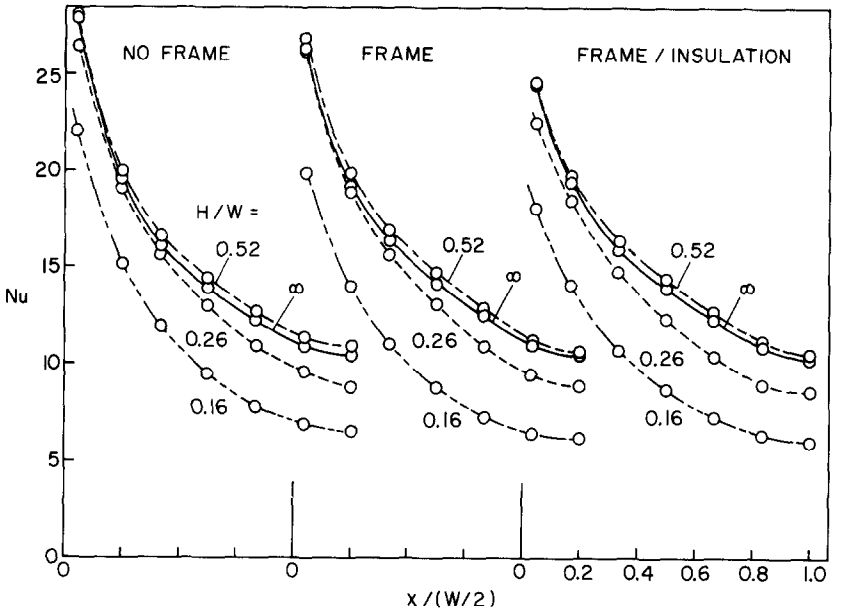

FIG. 6. Distributions of the local Nusselt number Nu ($\overline{Ra}^* = 6 \times 10^6$).

correspond to a specific mid-range $\overline{Ra}^*$ value of 6×10^6, the trends and relationships conveyed by the figure apply to all of the investigated $\overline{Ra}^*$.

The figure shows that, as expected, small gap heights cause significant reductions of the Nusselt number. However, the reductions readily diminish as the height is increased, as witnessed by the fact that the Nu values for $H/W = 0.26$ are about 30% larger than those for $H/W = 0.16$. Further increases in gap height cause only moderate changes in the Nusselt number. It is interesting to note that the Nusselt numbers for the $H/W = 0.52$ gap are slightly larger than those for the case when there is no upper wall ($H/W = \infty$). It may be conjectured that supplementary buoyancy induced by the radiation-heated wall of the gap contributes to this effect.

Average Nusselt numbers

The average Nusselt number results for the heated plate are presented in Fig. 7. The figure consists of three tiers which correspond, respectively, to the no-frame, and frame/insulation configurations. For each configuration, $\overline{Nu}$ is plotted as a function of the modified Rayleigh number $\overline{Ra}^*$ for parametric values of the dimensionless gap height H/W. The lines interconnecting the data are least-squares fits. In the range $H/W \geqslant 0.31$, the data are sufficiently intermingled so as to make it impractical to fit a separate curve for each H/W. Consequently, in that range, only a single curve, that for $H/W = \infty$, was fit.

Examination of the figure shows that, as expected, the average Nusselt number attains its lowest values at the smallest gap height and increases with increasing height. The increase is monotonic at the smaller heights. In the range $H/W \geqslant 0.31$, the data tend to cluster, but it appears that $\overline{Nu}$ attains a weak maximum at a gap height less than $H/W = \infty$. However, for any practical purpose, the average Nusselt number can be regarded as being independent of the gap height when $H/W \geqslant 0.31$, so that in this range, the presence or absence of the upper wall is immaterial. The overall increase of the Nusselt number, starting with the smallest investigated gap height and proceeding to the large-gap limit, is about 50%.

For the most part, the variation of $\overline{Nu}$ with $\overline{Ra}^*$ is logarithmically linear. The one exception, the case with $H/W = 0.16$ (smallest gap) and frame present, was repeated and the data confirmed. There is a general tendency for $\overline{Nu}$ to become less sensitive to $\overline{Ra}^*$ as the gap height increases (i.e. the curves tend to flatten). For the important limiting case of $H/W = \infty$ and no frame,

$$\overline{Nu} = 1.07(\overline{Ra}^*)^{1/6}. \tag{10}$$

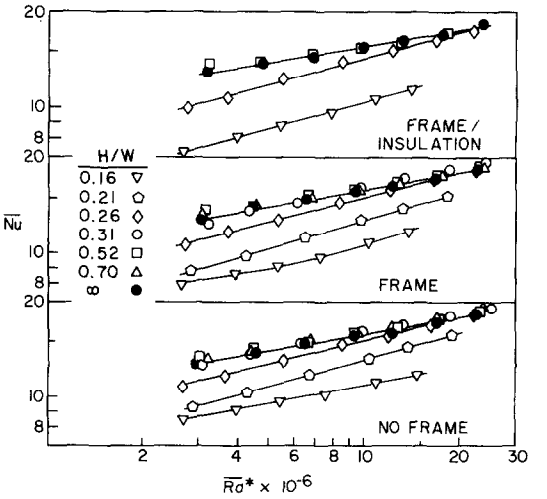

FIG. 7. Average Nusselt numbers $\overline{Nu}$.

As will be documented shortly, the 1/6-power dependence relates well with theoretical work for natural convection flow across a semi-infinite, uniformly heated horizontal plate.

Comparisons with literature

As was noted in the Introduction, there appears to have been no prior work for finite-gap heights, so that comparisons of the present results with the literature have to be limited to the case where there is no upper wall (i.e. $H/W = \infty$). The available analytical work deals with a semi-infinite heated plate—a plate whose only edge is at $x = 0$. The natural convection solution to this problem [4, 5] yields a boundary-layer flow which moves unidirectionally along the plate, from the edge toward larger x. In contrast, in the present experiments, the heated plate has edges at $x = 0$ and $x = W$, with the flow which originates at the former moving in the positive x-direction and the flow which originates at the latter moving in the negative x-direction. The collision of the two flows causes a plume to rise from the central region of the plate. The analytical solutions do not include a plume.

The uniform wall temperature and uniform heat flux boundary conditions were respectively analyzed in refs. [4] and [5]. After introducing the local Nusselt number defined by equation (4) and a local modified Rayleigh number

$$Ra^* = (g\beta q_x W^4/\nu^2 k)Pr \tag{11}$$

the $Pr = 0.7$ solution corresponding to the uniform heat flux boundary condition [5] takes the form

$$Nu/(Ra^*)^{1/6} = 0.553/(x/W)^{1/3}. \tag{12}$$

This equation is plotted in Fig. 8 along with the present $H/W = \infty$ no-frame data. The data correspond to six different values of $\overline{Ra}^*$ in the range between 4.5×10^6 and 2.3×10^7. Within plotting accuracy, the value of $Nu/(Ra^*)^{1/6}$ at a given station $x/(W/2)$ was found to be independent of $\overline{Ra}^*$. The thermophysical properties appearing in Nu and Ra^* were evaluated at the local film temperature.

In view of the aforementioned fundamental differences between the underlying physical problems, the agreement in evidence in Fig. 8 is unexpectedly good. The near-perfect accord adjacent to the $x = 0$ edge of the plate is as it should be, because the differences between the two problems should not be felt there. It is the faithful tracking of the data and the analytical curve in the central region of the plate (i.e. the plume region of the two-edged plate) which would not have been expected beforehand. The fact that the data fall above the curve can be attributed to the mixing caused by the collision of the two oppositely directed streams and to the fluid acceleration associated with the turning of the boundary layer into a plume.

The experimental information available in the literature for the $H/W = \infty$ case is limited to average Nusselt numbers for the uniform wall temperature boundary condition. The heat transfer data, as reported

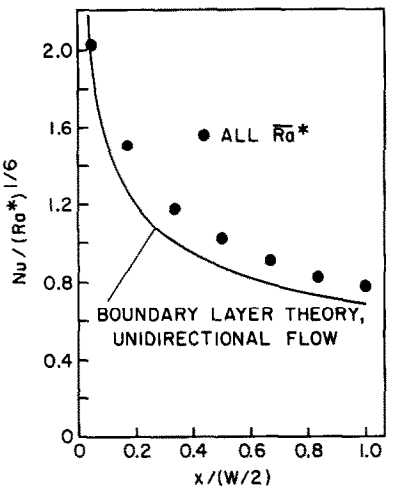

FIG. 8. Comparison of local Nusselt number data for $H/W = \infty$ with analytical predictions for a semi-infinite, uniformly heated plate.

in ref. [1], is for square or nearly square plates and is, therefore, unsuitable for comparison with those for the two-dimensional situation investigated here. Also, the data obtained by the naphthalene sublimation technique in [2] are not appropriate for comparison because they are limited to very low Rayleigh numbers. This leaves the results obtained by the electrochemical mass transfer technique as the remaining candidate for the comparison [3].

The correlation provided by [3] is a power-law relation between $\overline{Nu}$ and a Rayleigh number based on the plate-to-ambient temperature difference. To this end, a plate-average Rayleigh number $\overline{Ra}$ was evaluated as

$$\overline{Ra} = [g\bar{\beta}(\bar{T}_w - T_\infty)W^3/\bar{\nu}^2]\overline{Pr} \tag{13}$$

where, from equations (6) and (7), it follows that

$$\overline{Ra} = \overline{Ra}^*/\overline{Nu}. \tag{14}$$

The characteristic length in the aforementioned power-law correlation is the ratio of the plate surface area to its perimeter. The present experimental results correspond to two-dimensional conditions, so that the plate length cancels out of the area-to-perimeter ratio, yielding $W/2$. When this characteristic length is introduced, the correlation of [3] becomes

$$\overline{Nu} = 0.588\overline{Ra}^{0.255}. \tag{15}$$

Equation (15) is plotted in Fig. 9 (dashed line) along with a solid line which represents the $H/W = \infty$ no-frame results of the present experiments. As seen in the figure, the present results fall below equation (15) and well they should. It is well established in the modern heat transfer literature on natural convection [10, 11] that a Nusselt–Rayleigh relation does not fully account for the variations of the Prandtl number. In particular, at a fixed Rayleigh number, the Nusselt number increases as the Prandtl number increases. Since the results on which equation (15) are based correspond to

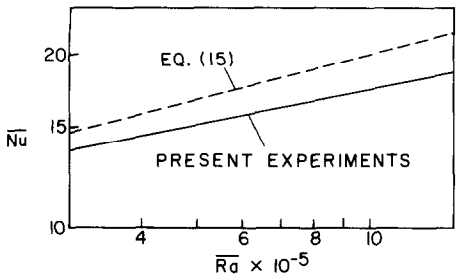

FIG. 9. Comparison of average Nusselt number data for $H/W = \infty$ with a correlation based on uniform-wall-temperature, high-Prandtl-number experiments.

$Pr \cong 2000$, while the present results are for $Pr \cong 0.7$, the positioning of the curves in Fig. 9 is proper.

Another possible contributing factor to the deviation of the two curves is that the area-to-perimeter characteristic length proposed in [3] may be only approximately applicable to two-dimensional situations. The modest difference in slope in evidence in the figure (0.200 vs 0.255) may be due to the different boundary conditions (uniform heat flux vs uniform wall temperature).

CONCLUDING REMARKS

The natural convection heat transfer characteristics of a uniformly heated, upward-facing, horizontal plate, shrouded by a parallel, adiabatic surface situated above the heated plate, were determined experimentally in air. Results were obtained for both the local Nusselt number Nu and the average Nusselt number $\overline{Nu}$. The heated plate and the shroud were strip-like rectangles of identical dimensions, and the experiments were conducted so that the flow was two-dimensional (i.e. no flow in the direction of the plate length). Experiments were also performed for the unshrouded heated plate, since it had not been previously investigated for the uniform heat flux boundary condition nor had local Nusselt numbers been determined for any boundary condition.

Three parameters were varied during the course of the research. These included the ratio of the gap height H to the plate width W, the dimensionless heating rate represented by the modified Rayleigh number $\overline{Ra}^*$, and the configuration of the surroundings. In one configuration, the surroundings were unobstructed (no-frame case). In another, the heated plate was framed by a coplanar adiabatic surface which prevented air from being drawn into the interplate gap from below. In the third configuration, supplementary insulation was placed beneath the frame and adjacent to the heated plate.

In general, special precautions were taken to minimize extraneous heat losses. An analysis of the radiative interchange, including specular reflections at the highly polished heated plate, was made to correct for the heat loss by radiation.

The local Nusselt number Nu was found to decrease significantly from the edge of the plate to the center of the plate width, with the Nusselt number at the edge being about three times that at the center. The distributions of $Nu/\overline{Nu}$ across the width of the plate were virtually independent of the heating rate $\overline{Ra}^*$, except at the smallest investigated gap height ($H/W = 0.16$) where a modest sensitivity to $\overline{Ra}^*$ prevailed. Furthermore, except for the smallest gap and adjacent to the plate edge for the other gap heights, $Nu/\overline{Nu}$ was insensitive to the configuration (no-frame, frame, and frame/insulation). In addition, for $H/W > 0.5$, the $Nu/\overline{Nu}$ distributions were independent of the gap height and, therefore, are universal with respect to all the parameters.

The unnormalized Nu distributions were depressed at small gap heights but rebounded rapidly as the gap height increased. There was little difference between the Nu distributions for $H/W \cong 0.5$ and for $H/W = \infty$ (i.e. no shroud surface).

The average Nusselt number $\overline{Nu}$ was also depressed at small gap heights but increased as the height increased. Between $H/W = 0.16$ and ∞, the increase in $\overline{Nu}$ was about 50%. For most practical purposes, $\overline{Nu}$ can be regarded as independent of the gap height when $H/W > \sim 0.3$.

REFERENCES

1. W. H. McAdams, *Heat Transmission*, 3rd edn. McGraw-Hill, New York (1954).
2. R. J. Goldstein, E. M. Sparrow and D. C. Jones, Natural convection mass transfer adjacent to horizontal plates, *Int. J. Heat Mass Transfer* **16**, 1025–1034 (1973).
3. J. R. Lloyd and W. R. Moran, Natural convection adjacent to horizontal surface of various planforms, *J. Heat Transfer* **96**, 443–447 (1974).
4. Z. Rotem and L. Claassen, Natural convection above unconfined horizontal surfaces, *J. Fluid Mech.* **39**, 173–192 (1969).
5. L. Pera and B. Gebhart, Natural convection boundary layer flow over horizontal and slightly inclined surfaces, *Int. J. Heat Mass Transfer* **16**, 1131–1146 (1973).
6. C. K. Carlson, Natural convection from a uniformly heated horizontal surface shrouded by a parallel equi-dimension plate. Thesis, Department of Mechanical Engineering, University of Minnesota, Minneapolis, MN (1984).
7. Santocel A Silica Aerogel, Technical Bulletin I-180, Monsanto Inorganic Chemicals Division, St. Louis, MO (1971).
8. E. R. G. Eckert and E. M. Sparrow, Radiative heat exchange between surfaces with specular reflection, *Int. J. Heat Mass Transfer* **3**, 42–54 (1961).
9. E. M. Sparrow, E. R. G. Eckert and V. K. Jonsson, An enclosure theory for radiative exchange between specularly and diffusely reflecting surfaces, *J. Heat Transfer* **84**, 294–300 (1962).
10. S. W. Churchill and H. H. S. Chu, Correlating equations for laminar and turbulent free convection from a vertical plate, *Int. J. Heat Mass Transfer* **18**, 1323–1329 (1975).
11. S. W. Churchill and H. H. S. Chu, Correlating equations for laminar and turbulent free convection from a horizontal cylinder, *Int. J. Heat Mass Transfer* **18**, 1049–1053 (1975).

NOMBRES DE NUSSELT LOCAUX ET MOYENS DE CONVECTION NATURELLE POUR UNE PLAQUE HORIZONTALE COUVERTE ET UNIFORMEMENT CHAUFFEE

Résumé—On décrit des expériences faites pour déterminer les caractéristiques du transfert thermique par convection naturelle pour une plaque horizontale tournée vers le haut, uniformément chauffée, couverte par une surface parallèle, adiabatique et située au-dessus d'elle. Trois paramètres variables sont la hauteur adimensionnelle de l'espacement (l'absence de couverture étant la limite supérieure), le flux de chauffage adimensionnel (nombre de Rayleigh) et la configuration de l'environnement (absence ou présence d'une obstruction et d'une isolation supplémentaire). L'air est le milieu de transfert thermique. Le nombre de Nusselt est le plus élevé au bord de la plaque chauffée et il décroit vers le centre, où il n'est là que le tiers de celui du bord. Les distributions du nombre de Nusselt local, normalisé par le nombre de Nusselt moyen, est universel (c'est-à-dire indépendant des paramètres) pour des espacements supérieurs à une valeur plancher. Les nombres de Nusselt locaux et moyens sont ensemble diminués par des faibles espacements mais ils croissent rapidement quand ils augmentent. Une hauteur critique est trouvée telle que pour les valeurs supérieures le nombre de Nusselt moyen est indépendant de la présence ou de l'absence de la couverture.

ÖRTLICHE UND MITTLERE NUSSELT-ZAHL BEI NATÜRLICHER KONVEKTION AN EINER GLEICHMÄSSIG BEHEIZTEN, HORIZONTALEN PLATTE MIT ODER OHNE ABDECKUNG

Zusammenfassung—Zur Bestimmung der örtlichen und mittleren Wärmeübertragungseigenschaften an der Oberseite einer gleichmäßig beheizten horizontalen Platte, oberhalb der sich eine dazu parallele adiabate Fläche befindet, wurden Versuche durchgeführt. Drei Parameter wurden bei den Versuchen variiert, die dimensionslose Höhe des Spaltes zwischen den Platten (der nicht überdeckte Zustand wird als obere Grenze angesehen), die dimensionslose Heizrate (Rayleigh-Zahl), die Konfiguration der Umgebung (ein zusätzliches Hindernis oder eine zusätzliche Wärmedämmung). Das wärmeübertragende Medium war Luft. Die örtliche Nusselt-Zahl war an der Kante der beheizten Platte am höchsten und nahm entlang der Plattenoberfläche bis auf ein Drittel des Maximalwerts in der Plattenmitte ab. Die örtlichen Nusselt-Zahlen wurden mit den korrespondierenden mittleren Nusselt-Zahlen normiert; dabei ergab sich, daß die örtliche Verteilung der normierten Nusselt-Zahlen ab einer bestimmten Mindestspalthöhe von den Parametern unabhängig ist.

ЛОКАЛЬНОЕ И ОСРЕДНЕННОЕ ЕСТЕСТВЕННОКОНВЕКТИВНЫЕ ЧИСЛА НУССЕЛЬТА ДЛЯ ОДНОРОДНО НАГРЕТОЙ, ЭКРАНИРОВАННОЙ ИЛИ НЕЭКРАНИРОВАННОЙ ГОРИЗОНТАЛЬНОЙ ПЛАСТИНЫ

Аннотация—Проведены эксперименты по определению характеристик локального и осредненного естественноконвективного теплопереноса для однородно нагреваемой горизонтальной пластины, обращенной нагреваемой стороной вверх, экранированной параллельной ей адиабатической поверхностью и расположенной над ней. В экспериментах изменялись три параметра: безразмерная высота зазора между пластинами (неэкранированный случай соответствует верхней оценке), безразмерная интенсивность нагрева (число Рэлея) и геометрия окружения (наличие или отсутствие преград и дополнительной изоляции). Теплопередающей средой служил воздух. Локальное число Нуссельта было наибольшим на краю нагреваемой пластины и уменьшалось вдоль ее поверхности; в центре оно составляло примерно одну треть от его величины на краю. Найдено, что распределения локального числа Нуссельта, нормированного по соответствующему осредненному числу Нуссельта, являются универсальными (т.е. независимыми от параметров) для высот зазора, больших порогового значения. Как локальное, так и осредненные числа Нуссельта уменьшались вместе с высотой зазора, но резко возрастали с его увеличением. Была найдена критическая высота зазора, такая, что для значений, превышающих ее, осредненное число Нуссельта не зависело от экрана.